A Numerical Study of Soil Confinement Effects on the Elastic Buckling of Large-Span Soil–Steel Bridges

Amer Wadi
Higher Colleges of Technology, UAE
awadi@hct.ac.ae (corresponding author)

Sokrates Ioannou
Higher Colleges of Technology, UAE
sioannou@hct.ac.ae

Yousef Alqaryouti
Higher Colleges of Technology, UAE
yalqaryouti@hct.ac.ae

Ahmed Alqarawi
Higher Colleges of Technology, UAE
aalqarawi@hct.ac.ae

Received: 9 March 2026 | Revised: 5 April 2026 | Accepted: 17 April 2026

 DOI: https://doi.org/10.48084/etasr.18621

ABSTRACT

The structural performance of soil–steel composite bridges is governed by the interaction between the corrugated steel shell and the surrounding soil, with elastic buckling being a key stability limit state. This effect occurs in all buried structures but becomes increasingly significant for large-span configurations under reduced soil confinement. This paper presents a numerical investigation of how soil cover influences elastic buckling behavior, using a consistent finite element eigenvalue analysis framework. A total of 45 cases, including several large-span structural profiles with varying corrugation stiffness and soil properties, were analyzed under both deep-burial and zero-cover conditions. Soil support was represented using a Winkler-type Spring model, with uniform stiffness for deep burial and depth-dependent stiffness for the zero-cover case to capture the loss of confinement near the crown. The results show that deeply buried structures follow a clear stiffness-controlled buckling trend, whereas shallow and zero-cover conditions lead to strong dependence on structural geometry and overall system flexibility. Based on these observations, an adjustment to existing elastic buckling formulations is proposed to better capture reduced confinement effects while remaining conservative relative to current design practice. The findings provide improved insights into elastic buckling behavior and support a more reliable and conservative stability assessment in practical design under shallow cover conditions, particularly for large-span soil–steel composite bridges.

Keywords-flexible culvert; soil–steel composite bridge; buckling; stability; soil–structure interaction; numerical analysis; large-span bridges

I. INTRODUCTION

Soil–Steel Composite Bridges (SSCBs) have been used as economical and efficient solutions for transportation infrastructure. Their structural behavior is governed by the interaction between the flexible corrugated steel shell and the surrounding compacted backfill. This composite action was established through the ring-compression theory presented in [1, 2], later developments in elastic foundation modeling [3, 4], and the early buckling formulations proposed in [5]. These concepts subsequently formed the basis of current design provisions [6-8]. The load-carrying capacity and buckling resistance of soil–steel systems depend on the effectiveness of the soil cover, which provides the confinement required to stabilize the flexible steel shell. Under live loading, the depth of soil cover above the crown influences how stresses are distributed within the backfill, thereby controlling the confining pressure that contributes significantly to structural performance

and buckling resistance. Experimental and field observations have shown that insufficient cover can reduce confinement, resulting in larger deformations and increased susceptibility to instability under surface loading [9-11]. Laboratory studies [12] further demonstrated that increasing the soil cover improves load distribution and shell stability, although the rate of improvement decreases at greater cover depths. Minimum cover requirements proposed for large-span structures also highlight the sensitivity of deformation and stability to burial depth [13, 14]. This is particularly relevant in modern practice, where increasingly larger spans are being constructed, including the 32 m span Guinness World Record SSCB structure in the UAE [15].

Concerns regarding shallow burial and elastic stability have been reinforced by studies addressing extreme loading conditions and structural deterioration [16-18]. Ultimate load tests and numerical simulations have shown that reduced soil cover can produce deformation patterns associated with the onset of buckling [9, 19]. Numerical investigations have also demonstrated that shallow cover increases bending effects and deformations under asymmetric loading, particularly in sloping terrain [11]. Since elastic buckling behavior is difficult to capture through physical testing alone, numerical modeling has become an essential tool for evaluating the relationship between soil cover and structural stability. Finite element studies have successfully reproduced full-scale structural behavior and have improved the understanding of how cover depth influences internal force distribution and deformation patterns [20-22]. Similar numerical methods have also been applied to broader soil–structure interaction problems, including ground anchors embedded in soil [23] and bridge foundation systems analyzed using finite element modeling combined with subgrade reaction approaches [24]. Nonlinear analyses extended to ultimate limit states further indicate that burial depth has a significant influence on both the initiation of buckling and the subsequent development of collapse mechanisms [16, 25].

Contemporary design provisions, including those in the Canadian Highway Bridge Design Code (CHBDC), American Association of State Highway and Transportation Officials (AASHTO), and the Swedish Design Method (SDM) [6-8], apply a limit-state design framework in which SSCBs are evaluated at both the Serviceability Limit State (SLS) and Ultimate Limit State (ULS). At SLS, attention is directed toward construction-induced deformations and the associated stresses within the steel plates, whereas ULS evaluation focuses on the combined action of axial force and bending moment together with the structure's resistance to buckling. The quality of the backfill and the depth of soil cover exert a strong influence on global stiffness, buckling calculations, and ultimate load-carrying capacity.

Most established design methods [3, 6, 8] use the Winkler idealization to estimate critical buckling resistance, in which the surrounding soil is represented by independent radial springs. AASHTO [8] additionally incorporates an elastic continuum solution [26] for the design of long-span culverts. The CHBDC and the SDM use formulations largely based on [3, 5], where buckling resistance is expressed as a function of soil cover depth and a reduced modulus representing soil stiffness. Early formulations assumed the effective thickness of the surrounding soil cylinder to be equal to the soil cover depth. This led to the unrealistic prediction of zero buckling resistance at the crown when the cover approached zero. Later refinements, discussed in the CHBDC commentary [27], addressed this limitation by adopting an average equivalent cover depth equal to half the distance between the crown and the spring line. This modification was subsequently incorporated into the 2006 edition of the CHBDC and was shown to significantly influence buckling predictions for large-span structures. The SDM, however, did not adopt this revision. In the present study, the Winkler representation is retained to remain consistent with the assumptions of current design methods, while allowing a clear assessment of soil confinement effects and a consistent comparison between deep-burial and shallow-cover conditions.

As spans continue to increase in modern SSCB applications, understanding the influence of soil cover on elastic buckling behavior has become important for evaluating current design approaches. Numerous studies have investigated culvert stability, ranging from simplified two-dimensional elastic models to advanced three-dimensional nonlinear analyses. However, there is still value in specifically isolating and quantifying the contribution of soil cover to buckling resistance within a consistent numerical framework for large-span SSCBs. Such an approach can provide benchmark data for calibrating simplified methods and improve the understanding needed to interpret more complex failure mechanisms. This study presents a systematic evaluation of the effect of soil confinement on elastic buckling behavior using a unified numerical framework. Unlike many existing approaches, the analysis isolates the role of confinement through direct comparison between deep-burial and zero-cover conditions across several large-span structural configurations. This allows a clearer assessment of the limitations of current design methods and supports the development of more reliable design formulations. Based on these findings, a practical modification within the SDM framework is proposed to better represent shallow-cover effects in design.

A. Aim and Scope

This study aims to investigate the elastic buckling capacity of SSCBs through a detailed numerical evaluation of selected structural configurations. The analysis is carried out using linear eigenvalue buckling procedures, in which the surrounding soil is represented by depth-dependent elastic springs, including the limiting case of zero soil cover. By examining two bounding conditions, shallow installation with no cover and deep burial with full confinement, the research quantifies the influence of soil cover on elastic buckling behavior. Beyond evaluating buckling capacity, the study seeks to improve the understanding of soil–structure interaction effects in SSCBs and to assess how existing design approaches reflect the numerical findings. The outcomes are intended to inform potential refinements to current design methodologies for elastic stability assessment in SSCBs.

II. METHODOLOGY

A. General

This study examines the influence of soil cover on the elastic buckling behavior of SSCBs. It builds on concepts discussed in the CHBDC commentary [27] by moving beyond simplified adjustments to equivalent spring stiffness and instead undertaking a systematic parametric evaluation of elastic buckling behavior across multiple large-span configurations. This approach enables the influence of soil confinement to be quantified within a consistent numerical framework. Using the Winkler model, the soil surrounding deeply buried structures is represented by uniform radial springs of equal stiffness distributed around the pipe circumference. In this context, deep-burial conditions are generally associated with soil cover heights greater than or equal to twice the pipe radius [26], where full confinement of the steel shell may reasonably be assumed. In contrast, the zero-cover condition reduces the available soil support above the crown, leading to lower radial spring stiffness in the upper portions of the structure. By comparing these two boundary cases, the study aims to quantify the reduction in elastic buckling capacity under zero-cover conditions relative to the same profile under deep burial. Although the Winkler model does not capture shear interaction within the soil mass or full continuum soil behavior, it remains well-suited for comparative and parametric assessment of confinement effects. It should also be noted that a zero-cover condition does not represent normal field practice, since design standards typically require a minimum soil cover to avoid undesirable failure mechanisms.

To achieve this, seven profile shapes were selected as shown in Figure 1, to represent different spans and height-to-span ratios, consistent with geometries typically used in industry practice [28]. For each case, eigenvalue buckling analysis using Abaqus [29] was employed to estimate the elastic buckling loads for both deeply buried and zero-cover scenarios. The soil support was represented using bidirectional springs. Unidirectional springs, which resist only compression, better reflect real soil behavior but cannot be used to compute elastic buckling loads because the geometric stiffness matrix cannot be formed. Therefore, the elastic buckling load was obtained using a bidirectional spring model, which provides stiffness in both directions solely to enable the eigenvalue analysis. Eigenvalue analysis provides only the elastic buckling load, as it is based on linear perturbations and does not capture inelastic or post-buckling behavior. Nonetheless, this approach is appropriate for capturing the influence of profile shape on elastic buckling and for quantifying differences between zero-cover and deep-burial conditions. The results of the simulated cases are also compared with existing buckling approaches from various relevant design methods.

For the deeply buried cases, the radial spring stiffness for the deep-burial condition, k_s, is calculated using the concept established in [3] and expressed in (1), where $E_{soil}$is the elastic modulus of the soil and $R_t$is the top radius of the structure. For the zero-cover condition, the radial spring stiffness is varied with depth according to (2), following the approach discussed in [27]. This expression defines the depth-dependent spring stiffness, $k_{s,depth}$, as a function of the vertical distance $y$measured from the crown. In the present study, the maximum spring stiffness is assumed to occur at the base of the structure, at a vertical distance $h$between the crown and the lowest point of the profile. Accordingly, the maximum stiffness $y = h$ is taken as k_s, representing the upper-bound stiffness within the adopted confinement profile. The depth-varying stiffness follows a sinusoidal-type distribution. The same reference stiffness, k_s, is used for the deep-burial case with uniform support, allowing direct comparison between the two conditions. Figure 2 illustrates the variation of $k_{s,depth}$with the vertical distance $y$from the crown.

$$k_s = (E_{soil}/R_t) \quad (1)$$

$$k_{s,depth} = k_s \times sin\left(\pi \frac{y}{2h}\right) \quad (2)$$

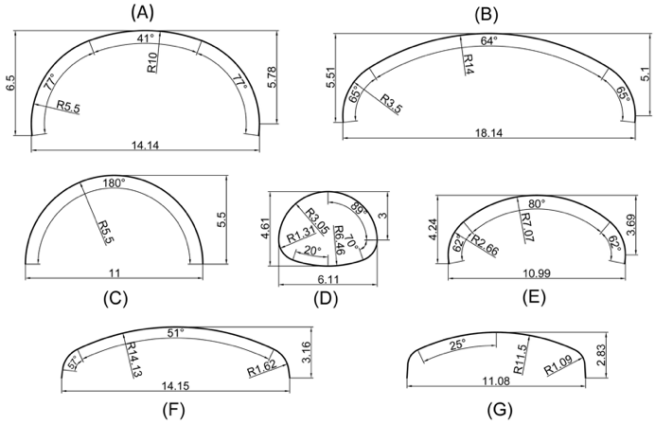

Fig. 1. Geometry of the selected profile shapes (m).

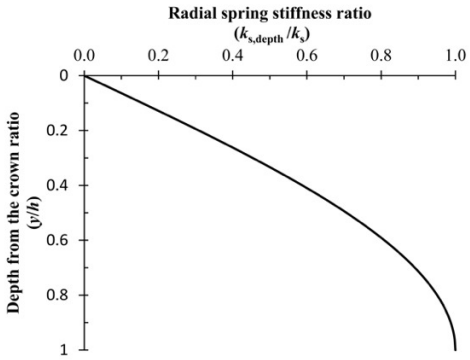

Fig. 2. Variation of spring stiffness with depth.

B. Simulated Case Studies

Seven profile shapes were selected, as depicted in Figure 1, to represent a range of spans and height-to-span ratios, including two cases representing box culverts. For each profile, different values of soil modulus and steel corrugations were applied. Three steel corrugation dimensions were assumed for the different cases as 500 mm × 237 mm, 381 mm × 140 mm, and 200 mm × 55 mm, as presented in Figure 3. Table I summarizes the 45 cases considered in the study, covering different profile shapes, a range of corrugation sizes, and

varying soil stiffnesses, with each case analyzed under both deep-cover and zero-cover conditions, resulting in a total of 90 simulations.

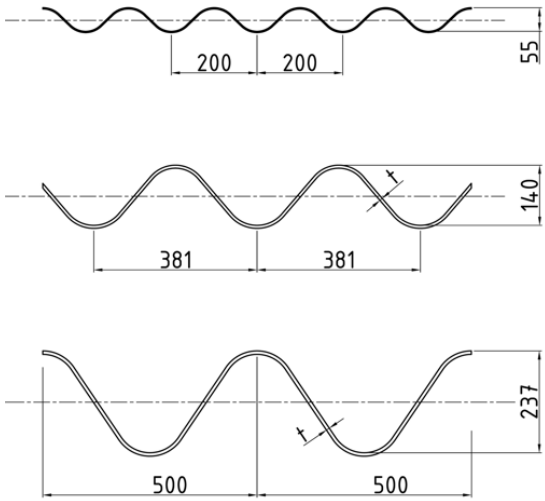

Fig. 3. Dimensions of the used steel corrugations.

TABLE I. INPUT PARAMETERS FOR ALL SIMULATED CASES

Profile shape	Corrugation size (mm)	Elastic soil modulus, E_{soil} (MPa)
A	381 × 140 × 7	10, 20 and 40
	381 × 140 × 5	10, 20 and 40
B	381 × 140 × 7	10, 20 and 30
	500 × 237 × 8	10, 20 and 40
C	381 × 140 × 7	10, 20 and 40
	381 × 140 × 3	10, 20 and 40
	200 × 55 × 7	5, 10 and 20
D	200 × 55 × 3	10, 20 and 40
	381 × 140 × 7	20, 30 and 40
E	381 × 140 × 7	10, 20 and 30
	200 × 55 × 7	5, 10 and 20
F	381 × 140 × 7	10, 20 and 40
	381 × 140 × 4	10, 20 and 40
G	381 × 140 × 7	10, 20 and 40
	200 × 55 × 7	5, 10 and 20

C. Numerical Simulation

The analysis was carried out in a 3D modeling environment to accommodate the explicit representation of the corrugated steel section. The steel wall was modeled using 3-node quadratic open-section beam elements (B32OS). The quadratic beam element was adopted to better represent the curved geometry and elastic buckling mode shape of the shell, while the open-section option was selected to remain consistent with the arbitrary profile definition used for the corrugated section in this study. The adopted element formulation was also checked through benchmark buckling analysis of a half-circle arch without soil springs, and the predicted critical load was found to be in good agreement with classical theoretical solutions for elastic buckling of circular arches [30]. The steel was assumed to be linear elastic, with a Young's modulus E of 200 GPa and a Poisson's ratio ν of 0.3. The corrugated steel geometry was represented explicitly using an arbitrary profile section definition, with the corrugation shape and plate thickness adjusted for each simulated case, as shown in Figure 4. A global mesh size of 0.1 m was adopted for all analyses, with curvature-based refinement and a minimum element size set to 10% of the global seed. A mesh sensitivity check was performed, and further refinement of the adopted mesh resulted in negligible changes in the predicted buckling loads. For the arch cases, the ends were modeled as pinned supports at the ground. For clarity, the main finite element modeling assumptions are summarized in Table II.

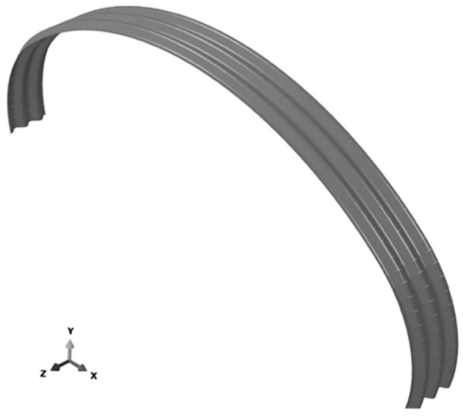

Fig. 4. An example of the visualized arbitrary profile section definition of the corrugation shape.

TABLE II. SUMMARY OF FINITE ELEMENT MODELING ASSUMPTIONS

Parameter	Description
Software	Abaqus 2023 [29]
Element type	B32OS
Geometry representation	Explicit corrugated profile (arbitrary section definition)
Steel model	Linear elastic steel (E = 200 GPa, ν = 0.3)
Soil model	Winkler springs (radial support)
Spring behavior	Bidirectional linear springs
Spring spacing	Approximately 0.5 m along the structure perimeter

The soil was modeled using the Winkler approach, represented by a series of linear elastic springs connected to nodes along the culvert perimeter and providing support primarily in the radial direction. For all profile cases, the springs were distributed at approximately 0.5 m arc-length intervals around the perimeter, as illustrated in Figure 5. The spring stiffness values for the deep-burial and zero-cover conditions were calculated using (1) and (2), respectively. For each case listed in Table I, an elastic buckling analysis was carried out for both boundary conditions: deeply buried and zero soil cover (Figure 5). The eigenvalue buckling analyses were performed by applying a uniformly distributed radial load along the circumference of the pipe or arch.

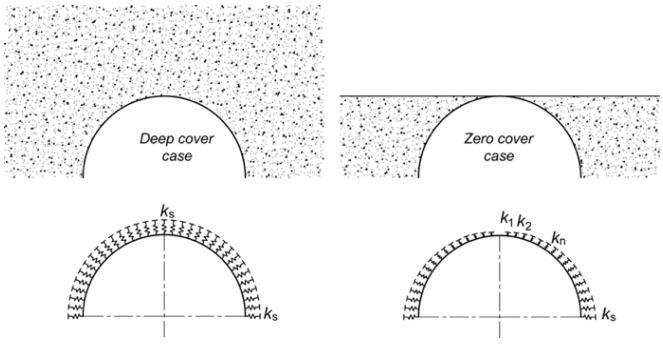

Fig. 5. A sketch showing the soil spring idealization for the two cases.

III. RESULTS AND DISCUSSION

A. Uniform Confinement Response

Figure 6 shows the elastic buckling load obtained from the Finite Element Method (FEM) analyses plotted against the parameter shown in (3) for the deep soil cover case (uniform springs). The linear trend observed in the results is consistent with the findings of earlier studies on the stability of soil–steel systems, as illustrated in (3) [5, 31, 32]. The results form a linear trend across all profiles, indicating that this simple stiffness-based parameter provides a good predictor of the elastic buckling capacity when uniform soil support is assumed. Despite the variation in corrugation size and profile geometry, the points from all seven profiles fall along the same regression line, suggesting that the influence of geometry is captured implicitly through the composite stiffness term.

$$N_{\mathrm{el}} = 2 \times \sqrt{\frac{E_{soil} \times EI_{steel}}{R_t}} \quad (3)$$

The scatter is small, with no significant deviation observed between profiles with different Rise-to-Span Ratios (H/D) (Distance between the crown and spring line / Span). This implies that, under deep soil cover, the buckling response is governed mainly by the combined soil–steel stiffness rather than by cover depth effects. Profiles with box shapes (G and F) fall higher on the trend line, but the proportionality remains consistent. Figure 6 also includes calculation results obtained using the elastic continuum approach in [26], which is adopted in AASHTO [8] for buckling checks of large-span culverts. While the continuum approach follows the general buckling trend, it exhibits greater scatter between profiles. This demonstrates that the current study, based on a Winkler Spring representation, explicitly captures the influence of structural geometry through the stiffness formulation, whereas the elastic continuum expression does not include a direct geometric scale parameter for the deep-burial case. The continuum equation in [8] is applied in the present work using only the scalar calibration factor Cn = 0.55, and without any reduction for soil cover, as it is intended for deep-burial conditions.

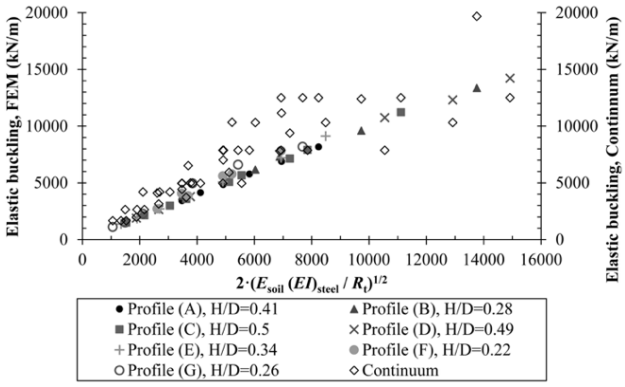

Fig. 6. FEM results for the elastic buckling under deep-burial conditions.

B. Zero-Cover Response

The zero-cover non-uniform spring results in Figure 7 show much greater scatter than the uniform case, with no single linear trend. Without crown confinement, the buckling response becomes strongly geometry-dependent, with profiles of lower H/D ratio exhibiting reduced elastic stability. This indicates that the simplified stiffness parameter is insufficient under zero-cover, as the response is governed by curvature distribution, corrugation size, and H/D. Moreover, in the zero-cover results, each profile separates into two or three clear linear trends, with each line corresponding to one corrugation size. Within each group, the buckling load increases linearly with the stiffness parameter, but the two/three lines are offset because the stiffer corrugation has a higher flexural stiffness of the corrugated steel shell (EI_{steel}). Across profiles, flatter and wider shapes (e.g., B, F) show lower buckling resistance, while more compact arches perform better, confirming that under zero-cover the response is governed jointly by corrugation stiffness and geometry. Figure 8 presents an example of the change in elastic buckling mode for Profile E when transitioning from deep burial to zero soil cover.

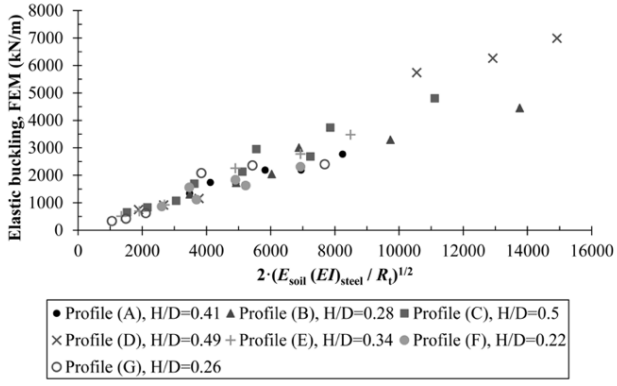

Fig. 7. FEM results for elastic buckling under zero-cover conditions.

(a) (b)

Fig. 8. An example of elastic buckling mode shapes for Profile E: (a) deep burial and (b) zero soil cover.

C. Geometric and Stiffness Sensitivity

Figure 9 illustrates the ratio of the zero-cover and deep-cover buckling loads for all simulated cases, plotted against H/D and the overall structural stiffness, denoted by the composite soil–steel stiffness parameter (λ_f). Deeper and more compact arches with larger H/D values (C, D) retain a higher proportion of their buckling capacity when the soil cover is removed. Flatter profiles with small H/D values (B, F, G) consistently show lower ratios, indicating a greater susceptibility to soil confinement. In addition, stiffer composite structures exhibit the highest ratios, confirming that stiffer configurations maintain much of their deep-cover capacity even under zero-cover. As stiffness decreases, the buckling ratio drops steadily, and the most flexible systems experience the largest reduction in capacity.

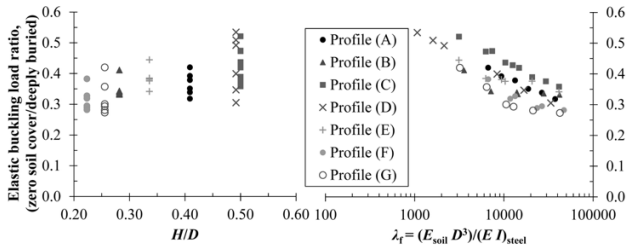

Fig. 9. Ratio between the zero-cover and deep-cover buckling loads for all simulated cases.

Moreover, Figure 10 demonstrates how both geometry (H/D) and λ_f influence the ratio between zero-cover and deep-burial buckling capacity. Higher H/D profiles retain a larger share of their deep-burial capacity, while increasing stiffness leads to a greater reduction under zero-cover conditions. The grey surface represents the fitted regression expression (4), which captures the numerical trends well ($R^2 = 0.85$):

$$Ratio_{red} = 0.18 + 0.3\frac{H}{D} + \frac{8.2}{\sqrt{\lambda_f}} \quad (4)$$

D. Development of a Buckling Modification Factor

Design standards typically treat shallow burial by reducing the elastic buckling capacity calculated for deep-cover conditions. This is done through two modifiers: an overall reduction factor that depends on the soil cover (ρ) (5), and a local reduction applied to the soil modulus for shallow to intermediate covers (ρ_{soil}) (6), as used in CHBDC [7]. Both factors are functions of the structure geometry H, R_t, and soil cover h_c. $N_{\mathrm{el,SDM}}$ is an elastic buckling force according to the SDM formulation. The SDM [6] adopts a similar formulation but without the $H/2$ term in both expressions, which leads to the elastic buckling resistance reducing to zero at zero soil cover.

$$\rho = \left(\frac{h_c + H/2}{R_t}\right)^{0.5} \leq 1 \quad (5)$$

$$\rho_{soil} = 1 - \left(\frac{R_t}{R_t + h_c + H/2}\right)^2 \quad (6)$$

$$N_{\mathrm{el,SDM}} = 1.2 \times \sqrt{\frac{E_{soil} \times EI_{steel}}{R_t}} \quad (7)$$

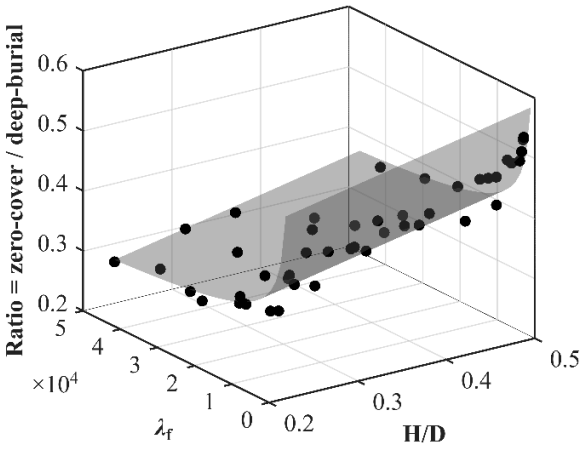

Fig. 10. Best-fit surface and numerical reduction factors for zero-cover buckling.

This work builds on the elastic buckling formulation currently used in the SDM, with emphasis on its treatment of shallow and zero soil cover. The objective is to propose a calculation that leads to ratios like those shown in Figures 9 and 10, when compared with elastic buckling forces calculated for deeply buried conditions using the SDM formulation, as given in (7). The aim is to introduce a modification factor F_b, applied to the vertical dimension H, similar in concept to the CHBDC reduction factor. This adjustment prevents unrealistically low elastic buckling predictions under shallow and zero-cover conditions while remaining consistent with the existing SDM design framework.

The results show that the proposed modification factor F_b in (8) varies systematically with both geometry H/D and system stiffness λ_f. The fitted expression captures the main trends observed in the numerical data and provides a practical means of adjusting the SDM elastic buckling calculation for shallow and zero-cover conditions. To remain consistent with current design practice, the value of F_b is capped at 0.5, in line with the upper limit adopted in CHBDC, preventing unrealistically high correction factors for very shallow or stiff cases. The proposed F_b factor is applied as a multiplier to H, thereby modifying the existing SDM calculation parameter κ_2 to (9).

$$F_b = \min\left[\left(0.58 - 0.51\left(\frac{H}{D}\right) + \frac{6.56}{\sqrt{\lambda_f}}\right), 0.5\right] \quad (8)$$

$$\kappa_2 = (h_c + F_b \times H)/R_t \quad (9)$$

Figure 11 presents the ratio between the proposed SDM modification to the CHBDC elastic buckling calculation for all simulated cases as evaluated at zero-cover. While the modified SDM approach removes the unrealistic drop to zero at zero covers, it consistently predicts lower buckling capacities than CHBDC across all profiles. This indicates that the proposed adjustment remains conservative, while providing a more realistic representation of buckling resistance under shallow and zero-cover conditions. CHBDC does not include buckling checks for box-type culverts (profiles F and G), and elastic buckling is evaluated using the ($R > R_e$) CHBDC formulation. Nevertheless, the comparison remains useful for highlighting relative trends across the studied geometries.

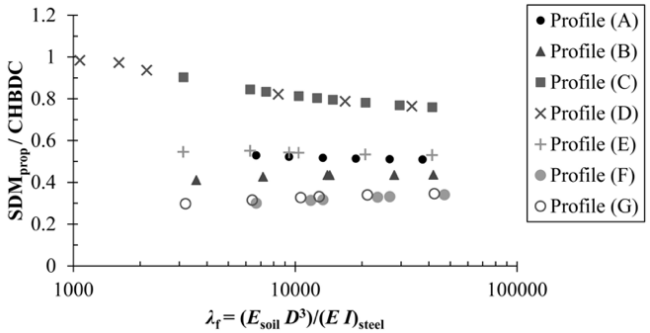

Fig. 11. Calculated ratio of elastic buckling capacity predicted by the proposed SDM modification to that predicted by CHBDC.

To demonstrate the effect of the proposed modification, Figure 12 presents a comparison between the modified SDM formulation, the current SDM approach, and the CHBDC elastic buckling equation for all simulated cases, assuming a soil cover of 1 m. The results show that the proposed modification consistently increases the predicted buckling resistance relative to the current SDM formulation, while generally yielding lower values than those obtained using the CHBDC equation. This comparison is not intended as a direct assessment of the relative performance of the two design methods. Rather, it serves as a comparative reference against existing design approaches, acknowledging that SDM and CHBDC employ fundamentally different design verification procedures, particularly in the treatment of the interaction between axial forces and bending moments.

Although the two design methods use different formulations for their respective checks, the comparison remains useful for assessing the proposed adjustment in relation to existing design approaches. From a practical design perspective, the proposed SDM modification improves second-order buckling calculations at shallow and intermediate cover depths, particularly for large-span structures, while remaining broadly consistent with other design approaches such as CHBDC.

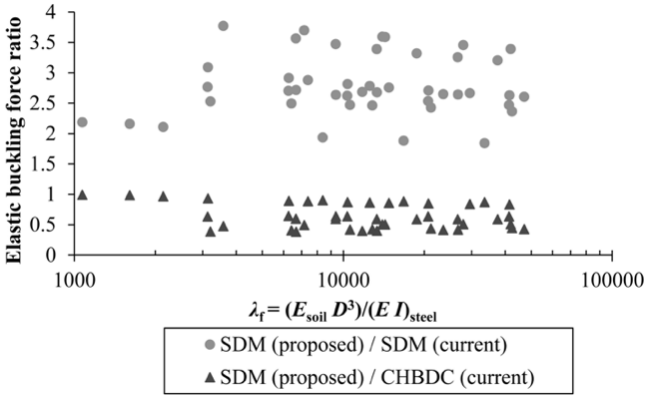

Fig. 12. Calculated ratios of elastic buckling capacity predicted by the proposed SDM modification relative to the current SDM formulation and CHBDC, for a soil cover of 1 m.

IV. CONCLUSIONS

This study investigated the influence of soil cover on the elastic buckling behavior of Soil–Steel Composite Bridges (SSCBs) using a consistent numerical framework. By comparing deeply buried and zero-cover conditions, the roles of soil confinement and structural geometry in governing buckling response were evaluated. The main findings and practical implications of the study are:

- Under deep-burial conditions, the elastic buckling capacity increases approximately linearly with the combined soil–steel stiffness parameter and shows limited dependence on profile shape.
- The elastic continuum approach follows the general buckling trend but exhibits greater scatter between profiles, since it does not explicitly account for geometric effects captured by the Winkler-based formulation adopted in this study.
- Shallow-cover conditions produce a strongly geometry-dependent buckling response. Flatter profiles with lower Rise-to-Span Ratios (H/D) ratios and more flexible soil–steel systems experience greater reductions in buckling resistance. The results indicate that the elastic buckling capacity under zero-cover conditions is typically about 30%–50% of the corresponding deep-burial capacity, depending on the geometry and structural stiffness.
- Introducing a modification factor within the SDM framework avoids unrealistically low predictions of elastic buckling resistance at shallow cover while remaining conservative relative to CHBDC.
- The proposed SDM adjustment improves second-order buckling estimates at shallow and intermediate cover depths and is particularly relevant for large-span structures, where buckling behavior is highly sensitive to changes in soil cover.

Future work could include a comparative evaluation of design outcomes obtained from different methods under shallow cover conditions to more rigorously assess differences

in predicted buckling capacity. Furthermore, nonlinear soil–structure interaction analyses, along with experimental validation, may be undertaken to further investigate post-buckling behavior and to support the refinement of future design recommendations.

DECLARATION OF COMPETING INTERESTS

The authors declare that they have no known competing financial interests or personal relationships that could have appeared to influence the work reported in this paper.

ACKNOWLEDGMENT

This research received no external funding. The work was carried out using computational and institutional resources provided by the university.

DATA AVAILABILITY

The data supporting the findings of this study are available from the corresponding author upon reasonable request.

SYMBOLS AND ABBREVIATIONS

The main symbols and abbreviations used in this study are summarized below:

- SSCB: Soil–steel composite bridge.
- H/D: Rise-to-span ratio.
- λ_f: Composite soil–steel stiffness parameter.
- k_s: Radial spring stiffness for deep-burial condition.
- $k_{s,depth}$: Depth-dependent radial spring stiffness.
- E_{soil} : Soil elastic modulus.
- EI_{steel}: Flexural stiffness of the corrugated steel shell.
- ρ: Reduction factor accounting for soil cover effects.
- ρ_{soil}: Reduction factor applied to soil stiffness.
- $N_{\mathrm{el,SDM}}$: Elastic buckling force according to the SDM formulation.
- R_t: Radius at the crown (top radius) of the structure.
- h: Vertical distance from the crown to the base of the structure.
- y: Vertical distance measured from the crown.
- F_b: Proposed modification factor for elastic buckling.
- H: Vertical dimension (distance between crown and spring line) of the structure.
- h_c: Soil cover height above the crown.
- κ_2: Calculation parameter.
- SLS: Serviceability Limit State.
- ULS: Ultimate Limit State.
- SDM: Swedish Design Method.
- CHBDC: Canadian Highway Bridge Design Code.
- AASHTO: American Association of State Highway and Transportation Officials.
- FEM: Finite Element Method.

REFERENCES

[1] H. L. White and j. P. Layer, "The corrugated metal conduit as a compression ring," *Armco Drainage and Metal Products*, vol. 39, pp. 389–397, Jan. 1960.

[2] M. G. Spangler and G. E. Shafer, "The structural design of flexible pipe culverts," *Iowa Engineering Experiment Station*, vol. 17, pp. 235–239, Jan. 1938.

[3] D. Glock and K. Klöppel, Theoretische und experimentelle Untersuchungen zu den Traglastproblemen biegeweicher, in die Erde eingebetteter Rohre. Technischen Hochshule Darmstadt, 1970.

[4] J. M. Duncan, "Behavior and Design of Long-Span Metal Culverts," *Journal of the Geotechnical Engineering Division*, vol. 105, no. 3, pp. 399–418, Mar. 1979, https://doi.org/10.1061/AJGEB6.0000777.

[5] G. Abdel-Sayed, "Stability of flexible conduits embedded in soil," *Canadian Journal of Civil Engineering*, vol. 5, no. 3, pp. 324–333, Sept. 1978, https://doi.org/10.1139/l78-037.

[6] L. Pettersson and H. Sundquist, *Design of soil steel composite bridges*. KTH Royal Institute of Technology, 2014.

[7] *Canadian highway bridge design code. CSA S6-25*. Ontario: Canadian Standards Association, 2025.

[8] *AASHTO Bridge Design Specifications*. USA: American Association of State Highway and Transportation Officials, 2020.

[9] E. B. Flener, "Response of Long-Span Box Type Soil-Steel Composite Structures during Ultimate Loading Tests," *Journal of Bridge Engineering*, vol. 14, no. 6, pp. 496–506, Nov. 2009, https://doi.org/10.1061/(ASCE)BE.1943-5592.0000031.

[10] E. Bayoglu Flener, "Testing the Response of Box-Type Soil-Steel Structures under Static Service Loads," *Journal of Bridge Engineering*, vol. 15, no. 1, pp. 90–97, Jan. 2010, https://doi.org/10.1061/(ASCE)BE.1943-5592.0000041.

[11] A. Wadi, L. Pettersson, and R. Karoumi, "Flexible culverts in sloping terrain: Numerical simulation of soil loading effects," *Engineering Structures*, vol. 101, pp. 111–124, Oct. 2015, https://doi.org/10.1016/j.engstruct.2015.07.004.

[12] V. T. Mai, I. D. Moore, and N. A. Hoult, "Laboratory Investigation of the Structural Performance of a Corrugated Steel Culvert under Increasing Cover Depth," *Journal of Bridge Engineering*, vol. 26, no. 6, June 2021, Art. no. 04021029, https://doi.org/10.1061/(ASCE)BE.1943-5592.0001722.

[13] M. Esmaeili, J. A. Zakeri, and P. H. Abdulrazagh, "Minimum depth of soil cover above long-span soil-steel railway bridges," *International Journal of Advanced Structural Engineering*, vol. 5, no. 1, Mar. 2013, Art. no. 7, https://doi.org/10.1186/2008-6695-5-7.

[14] T. J. McGrath and N. C. H. R. Program, *Recommended Specifications for Large-span Culverts*. Transportation Research Board, 2002.

[15] A. Wadi and R. Karoumi, "Estimation of live load deflections for soil-steel composite bridges," in *Bridge Maintenance, Safety, Management, Life-Cycle Sustainability and Innovations*, CRC Press, 2021.

[16] A. Wadi, L. Pettersson, and K. Raid, "FEM simulation of a full-scale loading-to-failure test of a corrugated steel culvert," *Steel and composite structures*, vol. 27, no. 2, pp. 217–227, Apr. 2018, https://doi.org/10.12989/scs.2018.27.2.217.

[17] I. Ezzeldin, H. El Naggar, and J. Newhook, "Performance of buried corrugated metal culverts in intact and deteriorated states under surface static loading utilizing full-scale laboratory tests," *Tunnelling and Underground Space Technology*, vol. 154, Dec. 2024, Art. no. 106099, https://doi.org/10.1016/j.tust.2024.106099.

[18] K. Lang *et al.*, "Nonlinear analysis of corrugated steel plate culverts using three-dimensional staged modelling under soil–steel interaction,"

Structures, vol. 79, Sept. 2025, Art. no. 109480, https://doi.org/10.1016/j.istruc.2025.109480.

[19] L. Pettersson, "Full Scale Tests and Structural Evaluation of Soil Steel Flexible Culverts with low Height of Cover," M.S. Thesis, Civil and Architectural Engineering Division of Structural Design and Bridges, Sweden, 2007.

[20] D. Beben and M. Wrzeciono, "Numerical analysis of steel-soil composite (SSC) culvert under static loads," *Steel and Composite Structures*, vol. 23, no. 6, pp. 715–726, Jan. 2017, https://doi.org/10.12989/scs.2017.23.6.715.

[21] Y. Liu, I. D. Moore, N. A. Hoult, and H. Lan, "Numerical Investigation of the Structural Behavior of Corrugated Steel Culverts under Surface Load Tests Using Three-Dimensional Finite-Element Analyses," *Journal of Pipeline Systems Engineering and Practice*, vol. 14, no. 2, May 2023, Art. no. 04023002, https://doi.org/10.1061/JPSEA2.PSENG-1412.

[22] A. Elsawwaf, H. El Naggar, and J. Newhook, "Effect of the employed soil constitutive model on the response of large-span soil steel bridges to soil and truck loading," *Journal of Constructional Steel Research*, vol. 228, May 2025, Art. no. 109436, https://doi.org/10.1016/j.jcsr.2025.109436.

[23] N. H. Al-Baghdadi, B. A. Ahmed, and A. N. Al-Jorany, "One-Dimension Finite Element Modeling of Grouted Ground Anchor," *Engineering, Technology & Applied Science Research*, vol. 12, no. 6, pp. 9752–9759, Dec. 2022, https://doi.org/10.48084/etasr.5325.

[24] H. Qiu, H. Wang, M. Ayasrah, Z. Zhou, and B. Li, "Study on Horizontal Bearing Capacity of Pile Group Foundation Composed of Inclined and Straight Piles," *Buildings*, vol. 13, no. 3, Mar. 2023, https://doi.org/10.3390/buildings13030690.

[25] Y. E.-A. Mohamedzein, "Nonlinear finite element analysis of load-deformation of soil-culvert systems," in *Geotechnics for Developing Africa*, CRC Press, 1999.

[26] I. D. Moore, "Elastic Buckling of Buried Flexible Tubes—A Review of Theory and Experiment," *Journal of Geotechnical Engineering*, vol. 115, no. 3, pp. 340–358, Mar. 1989, https://doi.org/10.1061/(ASCE)0733-9410(1989)115:3(340).

[27] *Commentary on CAN/CSA-S6-06, Canadian Highway Bridge Design Code.* Mississauga, Canada: Canadian Standards Association, 2006.

[28] Abaqus Analysis User's Guide. Dassault Systèmes, 2023.

[29] S. P. Timoshenko and J. M. Gere, *Theory of Elastic Stability*. Courier Corporation, 2012.

[30] U. Luscher, "Buckling of Soil-Surrounded Tubes," *Journal of the Soil Mechanics and Foundations Division*, vol. 92, no. 6, pp. 211–228, Nov. 1966, https://doi.org/10.1061/JSFEAQ.0000920.

[31] G. G. Meyerhof and L. D. Baikie, "Strength Of Steel Culvert Sheets Bearing Against Compacted Sand Backfill," *Highway Research Record*, no. 30, 1963.